Nuclear Inst. and Methods in Physics Research, A 903 (2018) 77–84

Contents lists available at ScienceDirect

Nuclear Inst. and Methods in Physics Research, A

journal homepage: www.elsevier.com/locate/nima

Characterization of atmospheric muons at sea level using a cosmic ray telescope

J.L. Autran *, D. Munteanu, T. Saad Saoud, S. Moindjie

Aix-Marseille Univ, Univ Toulon and CNRS, IM2NP UMR 7334, Faculté des Sciences, Service 142, Avenue Escadrille Normandie Niémen, F-13397 Marseille Cedex 20, France

ARTICLE INFO

Keywords:
Atmospheric muons
Cosmic rays
Muon flux
Muon telescope
Sea level muon intensity
Zenithal angle distribution

ABSTRACT

In this work, a portable cosmic-ray telescope was designed, assembled and operated to measure the cosmic-ray induced atmospheric muon flux at ground level. The instrument was entirely characterized and modeled from the point-of-view of detector efficiency, energy detection window and counting rate. Experimental data are reported for the characterization of the muon flux at sea level (43°N of latitude) in terms of vertical muon intensity and zenithal angle dependence.

1. Introduction

A large number of experimental works has been reported in the last decades on cosmic-rays muon intensities at sea level; these data are important for astrophysical standards and contain useful information concerning cosmic-ray interaction processes [1]. In a completely different field of interest, that initially motivated the present work, the metrology of terrestrial cosmic rays is also an essential challenge in modern microelectronics, for the understanding of basic mechanisms and for the characterization, modeling and predictive simulation of single event effects (SEE) in electronics [2]. SEE are radiation-induced errors in microelectronic circuits caused when energetic particles lose energy by directly (charged particles) or indirectly (neutrons) ionizing the medium through which they pass, creating electron–hole pairs at the origin of transient parasitic currents [3]. If the effort has so far focused mainly on the characterization of atmospheric neutrons [4–8], one must not longer neglect muons at ground level that are susceptible to significantly contribute to SEE in current integrated electronics [9–12]. Muons are indeed the most numerous energetic charged particles at sea level. They arrive at sea level with an average flux of about 1 muon per square centimeter and per minute. Their mean energy at sea level is ~4 GeV. For these typical energies and up to a few hundred of GeV, muons mainly interact with matter by ionization, losing energy at a fairly constant rate of about 2 MeV per g/cm^2. Although a large literature exists on muons in the atmosphere, studies are generally oriented "high energy physics" and consider muon energies above the GeV or beyond [11]. In the particular framework of radiation effects in microelectronics, there is an evident lack of data available in the "low energy" range, typically above a few tens of MeV and below a few GeVs. At these energies, muons can easily penetrate packaged ICs but are rapidly slowed or stopped: they can deposit by ionization a significant amount of electric charge along their track and contribute to single-event effects.

In the present work, we developed a cosmic-ray telescope to accurately characterize, in a long-term perspective effort, the atmospheric muon flux at ground level, precisely in this "low energy" range. This paper presents and discusses in details the main characteristics of the instrument and reports the experimental measurements conducted in the region of Marseille (south of France) at sea level.

2. The muon telescope

2.1. Experimental setup

In this work, we developed an experimental apparatus called "cosmic-ray telescope". Fig. 1 shows the front and back views of this setup derived from a real astronomical telescope fabricated by SkyVision (ultra compact Dobson, model 400-UT [13]). The initial telescope has been modified to receive two circular plastic scintillators (diameter 40 cm, thickness 5 cm, housed in 1.5 mm of aluminum plate) in place of the classical primary and secondary optical mirrors. This solution offers the advantage to take full benefits from an alt-azimuthal PC-controlled motorized mount with high precision mechanics and great

* Corresponding author.
E-mail address: jean-luc.autran@univ-amu.fr (J.L. Autran).

https://doi.org/10.1016/j.nima.2018.06.038
Received 11 February 2018; Received in revised form 3 June 2018; Accepted 11 June 2018
Available online 21 June 2018

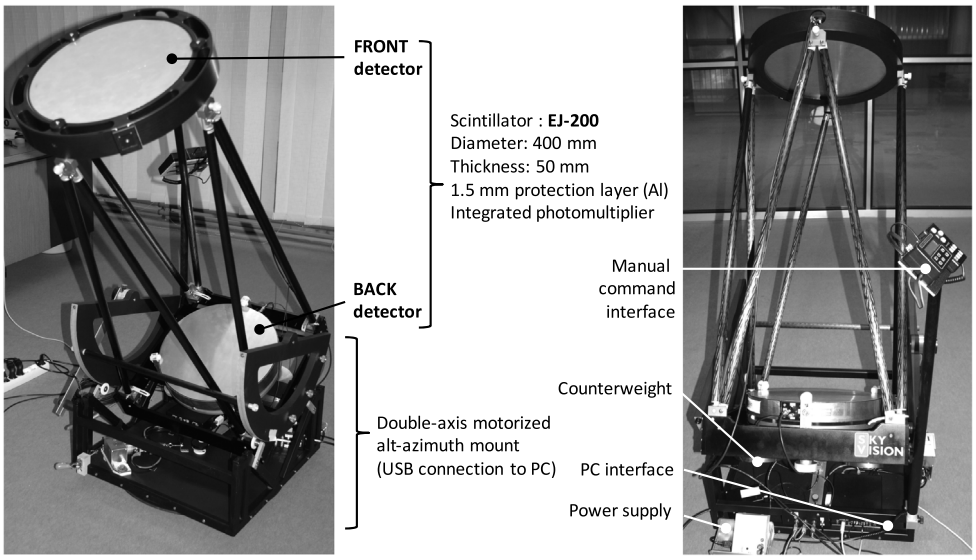

Fig. 1. Front and back views of the portable experimental setup (total weight 48 kg) composed of two circular scintillators (400 mm diameter) mounted in place of the primary and secondary mirrors of a real astronomical telescope with an alt-azimuthal double-axis motorized mount. The distance between the two scintillators is 102 cm.

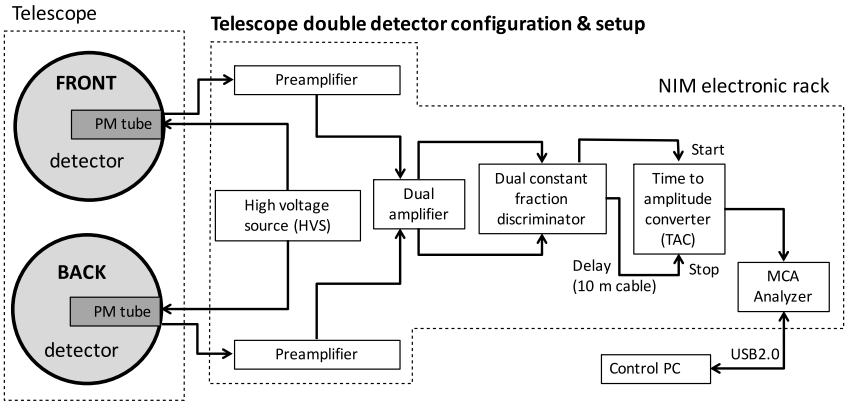

Fig. 2. Schematics of the electronics acquisition chain for measuring the time-of-flight of coincidence muons between the two detectors of the telescope.

transportability. The polymer base material of the two detectors is polyvinyltoluene (PVT) fabricated by Eljen Technology (EJ-200) [14]. This plastic is highly sensitive to charged particles: its typical stopping power for 1 GeV muons is 2.132 MeV/cm [15]. The two scintillators have photomultipliers (PM) directly integrated in their volume and optically coupled using a high refractive index optical coupling medium. The PMs are ADIT model PB29 with 1.125″ diameter, 2π photocathode and 11-stage photomultiplier. The assembly (PM + scintillator) is mounted in an aluminum housing (thickness 1.5 mm) that ensures a permanent light sealing. The two PMs are connected to the measurement and acquisition chain shown in Fig. 2.

The electronics chain trigs the muons traversing the front scintillator and measures, using a coincidence detection procedure, their time-of-flight between the front and back detectors separated by a distance of 1.02 m (in air). PM signals as well as time-of-flights converted in voltage pulses using a time-to-amplitude converter (TAC) are digitalized using multi-channel analyzers (MCAs based on 16k ADCs).

2.2. Instrument calibration

In order to be sure that the telescope detects and counts only atmospheric muons, a careful characterization and calibration of the instrument has been performed in several steps, described below.

2.2.1. Single detector characterization and γ rays rejection

In addition to muons, the two scintillators coupled with PMs of the telescope detect gamma rays, which are particularly present at low incident energy. Fig. 3 shows the telescope counting rate as a function of the MCA channel number. This curve shows two peaks: (i) a first low-energy peak that consists of a mixture of PM noise and the contribution of ambient gamma radiation; (ii) a second peak corresponding to the contribution of charged atmospheric muons. Note that the integral of this second peak (1200–1300 counts/min) corresponds perfectly to the product of the surface of the detector (1256 cm^2 in this case) with the integrated average muon flux at ground level (about 60 muons per square centimeter and per hour), demonstrating that this second peak is due almost exclusively to the contribution of muons in the count rate. In order to minimize the influence of gamma rays in measurements, a detection threshold of approximately 130 mV (corresponding to ADC channel 3500) was considered, as shown schematically in Fig. 3. Since this threshold is very dependent on the PM tube, a threshold value has been separately determined for each of the two (front and back) telescope detectors.

2.2.2. Detector efficiency

The raw counting rate of the telescope needs to be corrected to take into account the detection efficiency of both front and back

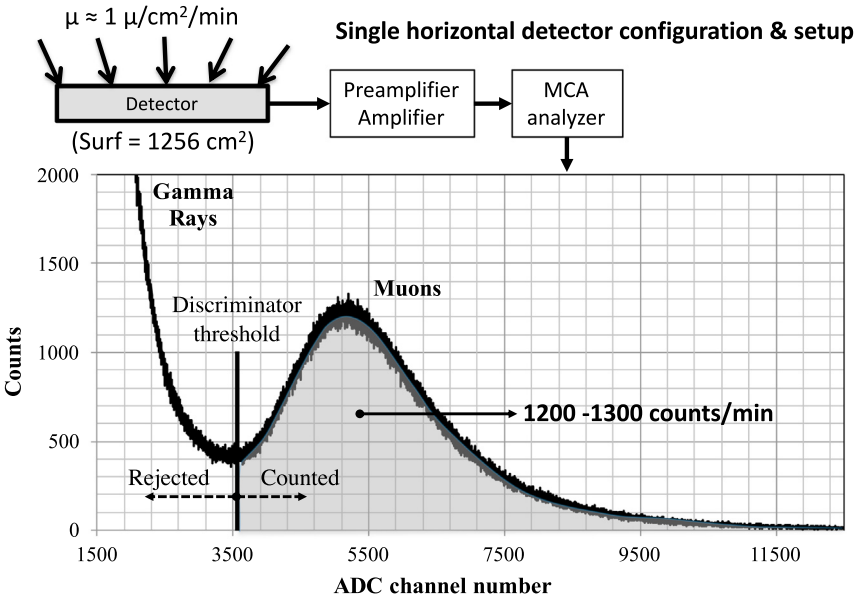

Fig. 3. Single detector acquisition chain used for fine-tuning the discrimination threshold in order to reject the gamma ray background. After threshold calibration, the counting rate of a single horizontal detector is 1200–1300 counts/min, that corresponds to approximately 60 particles per cm^2 and per hour.

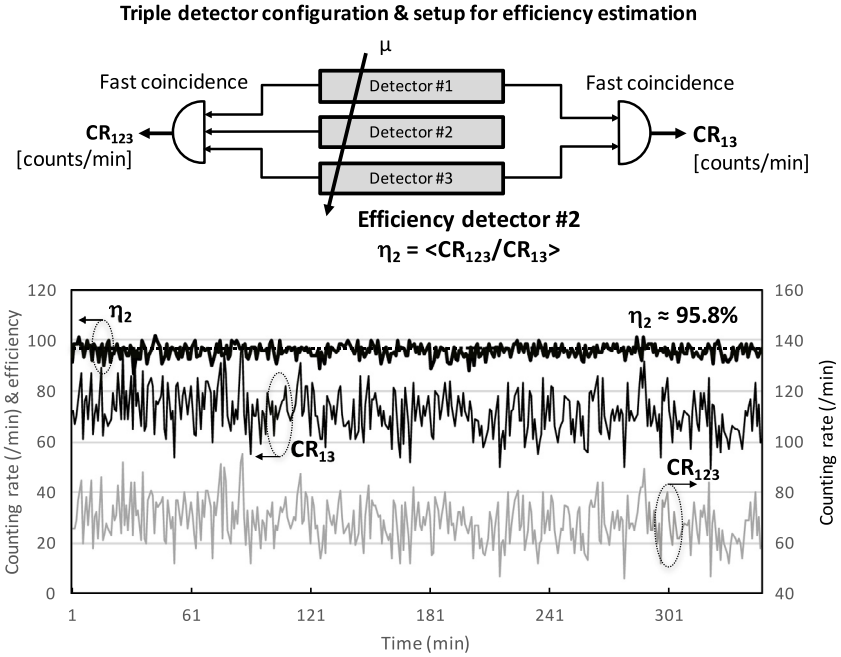

Fig. 4. Schematics of the electronics acquisition chain for measuring the detector efficiency. The detector to characterize (#2) is surrounded by two additional detectors (#1 and #3) used to count muons traversing the detector stack with and without the contribution of detector #2 in the coincidence counting rates, respectively noted CR_{123} and CR_{13}.

detectors since these sometimes do not detect a passing muon. For each detector, the detection efficiency is obtained by calculating the ratio between the number of detected particles and the number of incident particles effectively passing thought the bulk scintillator. To do this, we performed a coincidence measurement using three stacked detectors, as shown in the diagram of Fig. 4 (top). The detector #2 to be characterized is placed between two other detectors (#1 and #3) and the system measures, over a certain time interval, the number of events detected in coincidence, CR_{13}, between the detectors #1 and #3. Thus, if a muon is detected by #1 and #3 in coincidence, it has necessarily crossed the scintillator #2. At the same time, the system therefore measures the number of coincidences, CR_{123}, between detectors #1, #2 and #3. The efficiency of the detector to be characterized, η_2, is therefore given by:

$$\eta_2 = CR_{123}/CR_{13} \quad (1)$$

The efficiency of the two detectors of the telescope was estimated using this procedure. Fig. 4 (bottom) shows the variation with time of CR_{13}, CR_{123} and η_2 for the front detector. From these results, the measured detection efficiency of the telescope was estimated at η_F = 95.8% and η_B = 96.0% for the front and back detectors respectively (Fig. 4). The measured values remain constant over time, as shown in Fig. 4 for the front detector, and have been taken into account in the correction of all the experimental results.

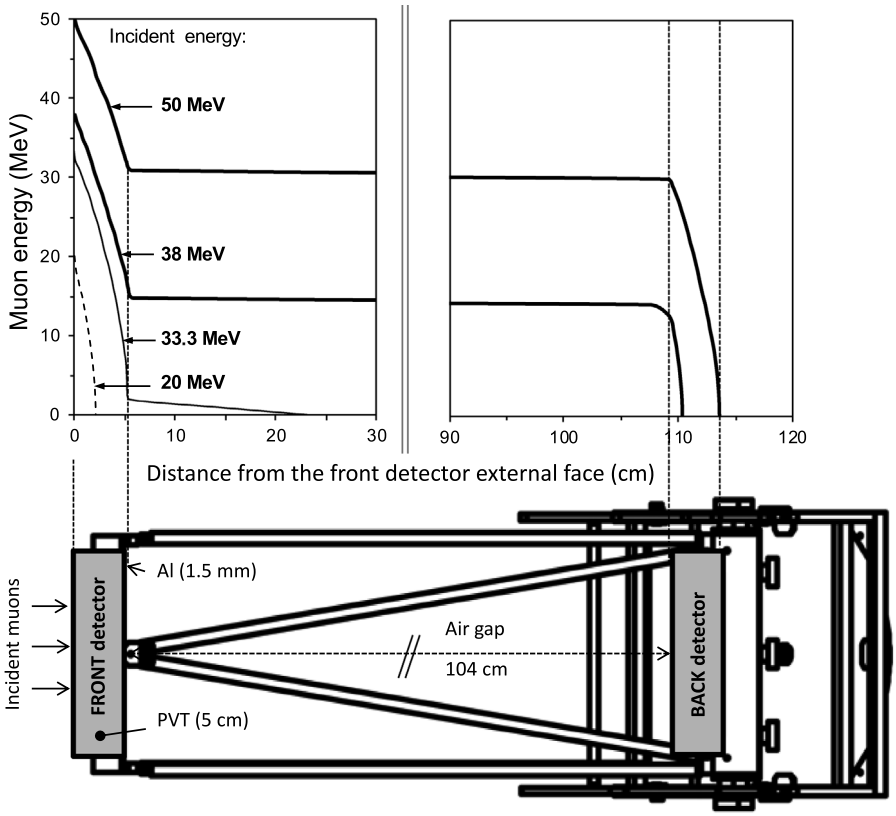

Fig. 5. TRIM simulations showing the slowing and stopping of muons in the telescope as a function of their incident energy (particle tracks perpendicular to the detector surfaces).

2.2.3. Electronic chain calibration

A calibration procedure has been preliminary performed to determine the MCA channel number versus time proportionality. The MCA was calibrated to a resolution of approximately 160 bins/ns. From time-of-flight distributions (not shown) of incident muons in the vertical direction for two detector distances of 25.5 cm and 104 cm, we deduced the average speed of cosmic ray muons, $v_\mu = 29.5 \pm 2.1$ cm/ns, i.e. 98.4% of c, in perfect agreement with the accepted value of $0.98 \times c$ [15].

2.3. Telescope modeling and simulation

2.3.1. TRIM simulation

In order to determine the minimum energy of muons that can be detected by the telescope, we performed extensive simulations using the TRIM (Transport of Ions in Matter) Monte Carlo simulation code [16]. In these simulations, we considered the exact 1D stack of materials traversed by incident muons during their passage through the instrument. Muons have been emulated in TRIM by applying a simple "mass scaling" to protons, as suggested in [17]. Fig. 5 shows the average distance traversed by muons in the instrument (perpendicular tracks) as a function of their incident energy. If muons with incident energies up to about 33 MeV are stopped in the front detector, higher energetic particles can reach the back detector and completely cross it above 50 MeV. Estimating that a particle depositing around 2 MeV in the scintillator material can be detected by the PM, the setup is thus able to detect incident muons above $E_{min} = 38$ MeV, which corresponds to the low energy cut-off of the instrument for particle tracks perpendicular to the detector. This value should be slightly higher for oblique tracks.

2.3.2. Counting rate modeling of the telescope

In a second step, the telescope counting rate has been numerically estimated from a model directly derived from the work of Sanderson and Page [18] in the case where the telescope is rotating under an anisotropic distribution of particles. Fig. 6 introduces the notations used in the following.

For an anisotropic distribution of incident muons I (m^{-2} s^{-1} sr^{-1}), the counting rate CR (s^{-1}) of the telescope pointing in the zenithal direction θ_d can be expressed as [18]:

$$\mathrm{CR}(\theta_d) = \eta_F \eta_B \int_0^{\Phi_m} \int_0^{\theta_m} S(\theta)\, I(\theta, \Phi) \sin\theta \cos\theta d\theta d\Phi \quad (2)$$

where η_F and η_B are the front and back detector efficiencies, respectively, θ_m is the acceptance angle of the telescope, S is the intersection of the projected shadow area of the front detector within the plane surface of the second detector [19] and Φ_m is the maximum value of the azimuthal angle for counting particles coming from the upper hemisphere [18].

$\Phi_m = 2\pi$ for a telescope pointing vertically ($\theta_d = 0$). For $\theta_d > 0$ and if $\theta + \theta_d > \pi/2$, the integration over Φ must be stopped at the angle Φ' where Φ' is given by:

$$\Phi' = \frac{\pi}{2} + sin^{-1}(cot\theta cot\theta_d) \quad (3)$$

For a cylinder-shaped telescope with two parallel and circular detectors of same radius R separated by the distance ℓ, as represented in Fig. 7, the intersection surface S (cross-hatched area) is given by Thomas and Willis [19]:

$$\mathrm{S}(\theta) = 2R^2 \arccos\left(\frac{\ell \tan\theta}{2R}\right) - \ell \tan\theta \sqrt{R^2 - \left(\frac{\ell \tan\theta}{2}\right)^2} \quad (4)$$

If we suppose in addition that the muon flux intensity susceptible to be detected by the telescope ($E_{min} > 38$ MeV) in a given arbitrary direction (vector OB, see Fig. 6) only depends on the zenithal angle θ' following a power cosine law, we can write:

$$I(\theta') = I_0 cos^n(\theta') \quad (5)$$

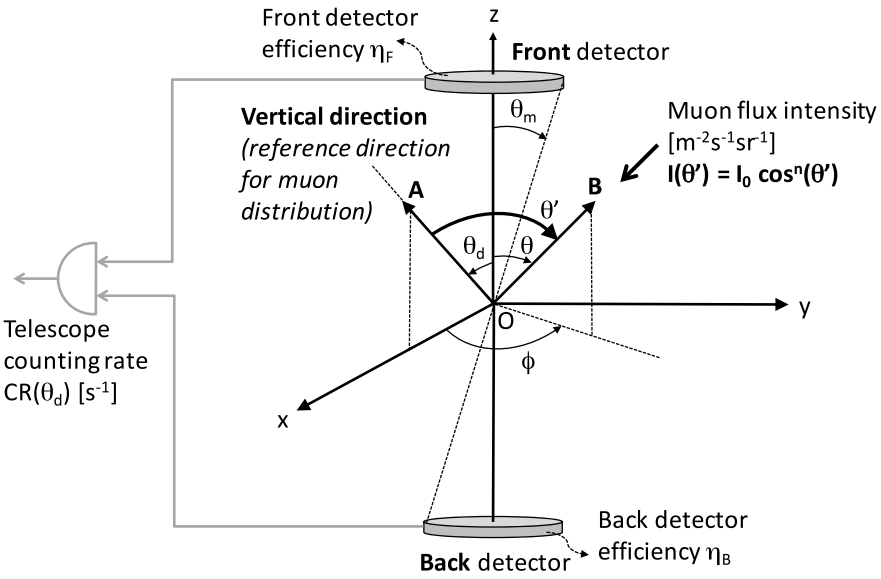

Fig. 6. Definition of axes, angles and other quantities used for the evaluation of the telescope counting rate when the distribution is rotated about the instrument. (Ox, Oy, Oz) is fixed with respect to the detector, OA is the reference direction of the muon distribution (vertical direction of the site), and OB is an arbitrary vector. For the instrument, the acceptance angle is $\theta_m = 19°335$.

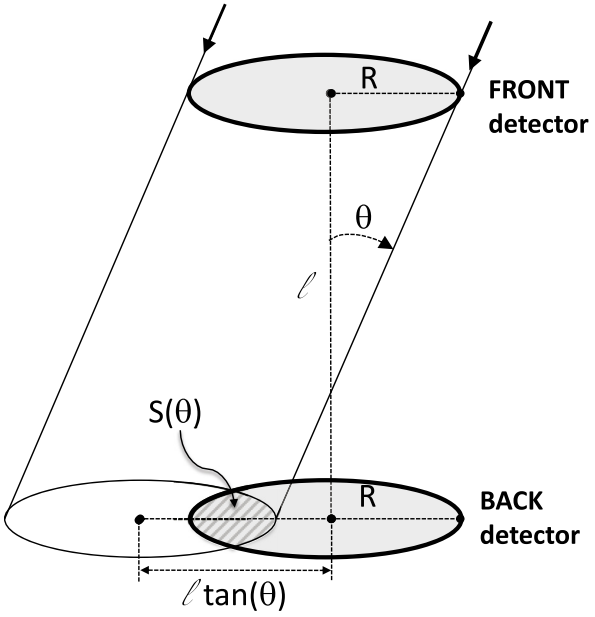

Fig. 7. Geometrical model used to derivate Eq. (2) from the "shadow area" approach described in Ref. [19].

where I_0 is the vertical muon flux (expressed in m^{-2} s^{-1} sr^{-1}) in the reference direction of the muon distribution (vector OA, see Fig. 6) and n is a real parameter.

In the general case depicted in Fig. 6, the angle between vectors OA and OB (an arbitrary vector) is [18]:

$$\cos\theta' = cos\theta cos\theta_d + sin\theta sin\theta_d cos\phi \tag{6}$$

Eq. (6) reduces to $\theta' = \theta$ when the telescope is pointing vertically (in this case, the z-axis attached to the telescope coincides to the reference direction OA of the muon distribution). In this particular case only, Eq. (2) reduces to [18,20]:

$$CR^V(\theta_d) = 2\pi \times \eta_F \eta_B \int_0^{\theta_m} S(\theta)\, I(\theta) \sin\theta \cos\theta d\theta \tag{7}$$

where CR^V (s^{-1}) is the vertical counting rate of the telescope.

The numerical integration of Eq. (2) using Eqs. (3)–(6) over the acceptance angle of the telescope allows us to estimate the telescope counting rate in the zenithal direction θ_d for any given values of I_0 and n, the two unknown quantities of this set of equations.

3. Experimental results: sea level measurements

Measurements have been performed outdoors on the Aix-Marseille University campus of Saint-Jérôme (Marseille, France, +43.338°N, +5.412°E, altitude 118 m) and on the roof of the Cassis's conference center (Cassis, France, +43.213°, +5.537°E, altitude 7 m). For the two measurement locations, the telescope was installed on a horizontal concrete slab during non-rainy days (Fig. 8 left). A control software has been developed to automatically perform the complete scanning over the solid angle (2π) or a partial scanning for fixed azimuthal or zenithal angle. The software also controls the integration time, timestamps all measurements and transfer data on the laboratory server for post-treatment.

To obtain additional values of the vertical counting rate as a function of the separation distance between the front and back detectors, a plastic resin shelf with seven regularly spaced shelves was also used in place of the telescope setup (Fig. 8 right). In this case, the two detectors were temporarily removed from the telescope bracket and aligned vertically on two shelves of this complementary characterization setup.

3.1. Vertical muon intensity

Measurements have been firstly performed with the telescope pointed in the vertical direction. A stable counting rate of 78 counts/min was measured over several days. Considering the acceptance angle of the instrument defined in Fig. 6 ($\theta_m = 19,335°$), this counting rate roughly corresponds to a vertical muon intensity $I_0 \approx 100$ m^{-2} s^{-1} sr^{-1}, in very good agreement with vertical flux values reported in literature at this latitude for energy muons ~3 GeV [21].

To check the validity of the telescope counting rate model described in Section 2.3.2 Eq. (7), we performed measurements in the vertical direction as a function of the separation distance between the front and back detectors using the additional setup (plastic shelf) described above. Fig. 9 shows the results of the model characterization: the values (represented in both linear and semi-logarithm scales) are in very good

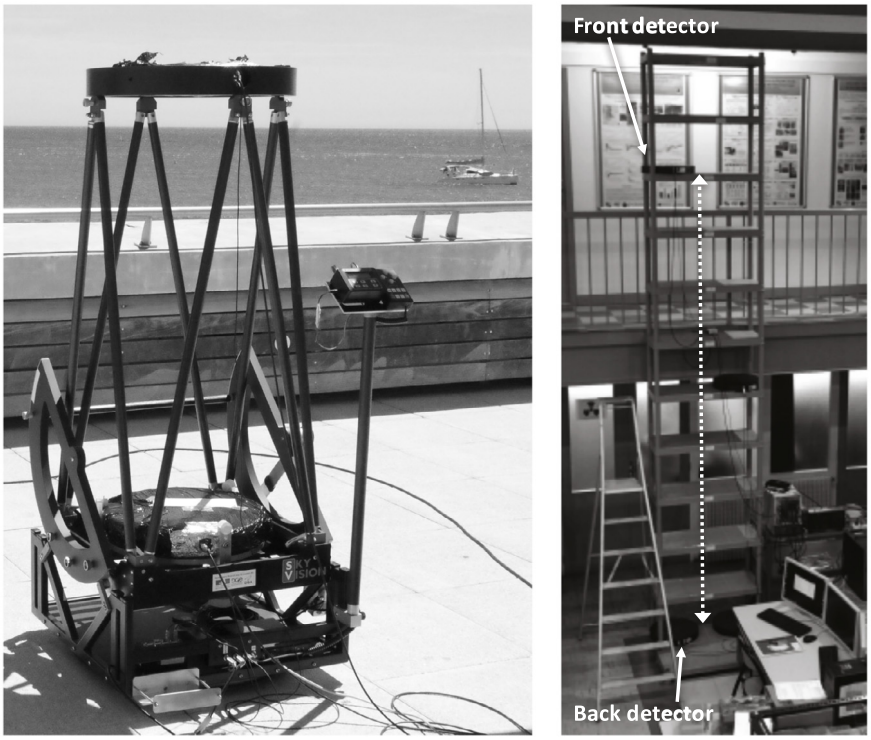

Fig. 8. (Left) The muon telescope outdoors in Cassis (France) at sea level; (right) An additional setup based on a plastic resin shelf used to characterize the counting rate in the vertical direction as a function of the distance between the two detectors.

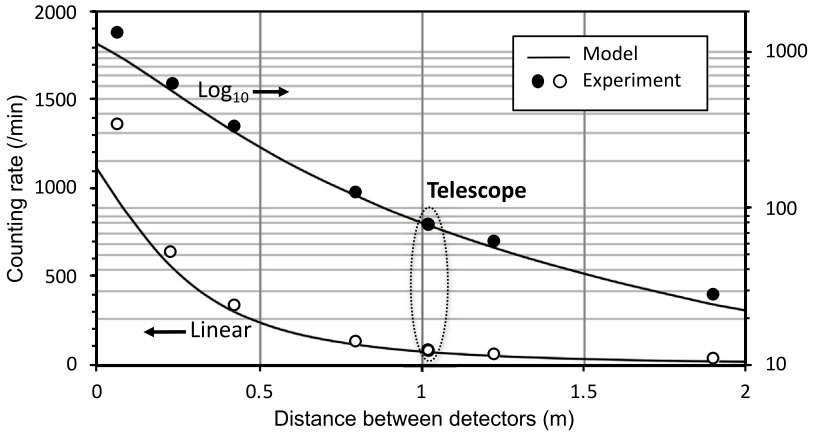

Fig. 9. Counting rate in the vertical direction as a function of the separation distance between the front and back detectors using the additional setup (plastic shelf) described in Fig. 8. The experimental points labeled "telescope" correspond to values measured using the telescope setup (distance of 1.02 m between the detectors). Simulated curves labeled "model" have been obtained from Eq. (2) to (5) with $n = 2$ and $I_0 = 100$ m^{-2} s^{-1} sr^{-1}.

agreement in a distance range between 10 cm and 2 m with the results of simulation using the numerical model presented above (Eq. (7) with $n = 2$ and $I_0 = 100$ m^{-2} s^{-1} sr^{-1}, see Section 3.2).

3.2. Angular distribution of muons

Fig. 10 shows the variation of the counting rate per minute of the telescope. Each point corresponds to a value averaged over one hour. This experimental counting rate data as a function of zenith angle measured using this specific telescope can be well fitted by a cosine power law with $n = 2.0 \pm 0.1$. This value is in coincidence with the value generally reported in the literature for the zenith angular distribution of muon flux with muon energy of ~3 GeV [21].

If we consider now the numerical model developed in Section 2.3.2 (Eqs. (2)–(6)), this model also perfectly fits experimental values of Fig. 10 when tuning I_0 and n parameters respectively to values $I_0 = 100$ m^{-2} s^{-1} sr^{-1} and $n = 2.0$. Additional curves in Fig. 10 calculated for $n = 1.9$ and $n = 2.1$ are also plotted (always for $I_0 = 100$ m^{-2} s^{-1} sr^{-1}). These curves graphically illustrated the sensitivity of the model to this parameter and allow us to roughly estimate the uncertainty on the determination of $n = 2.0 \pm 0.1$.

These results should be compared with those of Lin et al. [22] since both the experimental and the simulation approaches are similar. In the Lin et al.'s paper, the counting rate of the telescope (composed of two plastic scintillator plates, each with dimensions of 200 cm^2 in area, mounted in parallel with a separation distance of 1 m or 10.8 cm) is expressed by an integral equation of the zenith angular response function of the telescope folded with the zenith angle differential muon flux over the solid angle of the hemisphere assuming an isotropic azimuthal angular distribution of the muon flux. The zenith angular

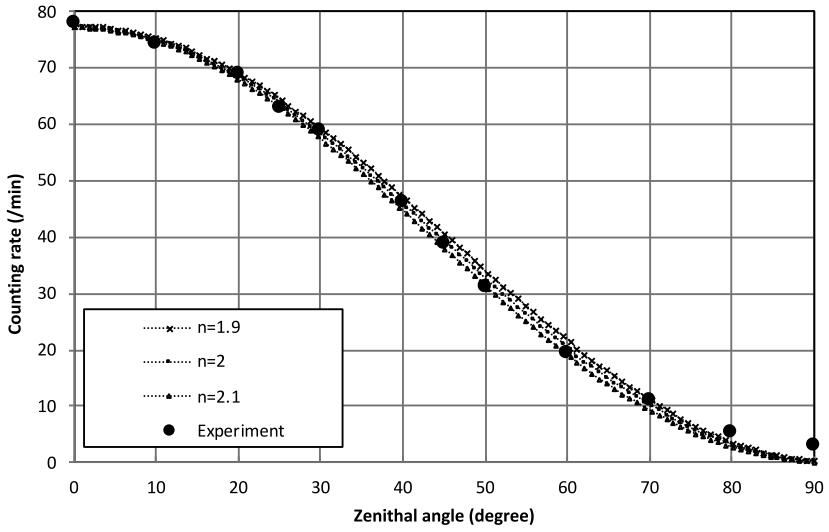

Fig. 10. Telescope counting rate (per minute) as a function of the zenithal inclination angle measured in the East direction (full dots). The best fitting curve for the raw measurements is obtained for $I_0 = 100$ μm^{-2} s^{-1} sr^{-1} and $n = 2.0$ (full line).

distribution of the muon flux was estimated by both the unfolding and the parameter adjusting methods, where the zenith angular response functions of the telescope were calculated using a Monte Carlo code, from the set of counting rates of the telescope measured at zenith angles from 0° to 90°. The angular distribution of muon fluence rate was determined to be close to a cosine power law with $n = 1.74$ for a separation distance between detectors of 1 m and $n = 1.21$ for a distance of 10.8 cm. Authors suggest that such differences may be induced by [22]: (i) a detection efficiency that depends of separation distance of the two scintillator plates (no energy attenuation in the scintillator plate has been taken into account, which may induce count-overestimation for the shortest separation distance) and (ii) a contribution to the telescope counting rate of an appreciable number of cosmic-rays electrons for which the angular distribution is different from that of high-energy muons. In the present case, results obtained with our telescope should not be concerned by these two limitations since: (i) the separation distance is large (1.02 m) and (ii) both detectors and electronic chain have been calibrated (see Section 2.2) to reject low energy particles. The result is a significantly higher coefficient n than reported by Lin et al. and close to the value $n = 2.0$ that is generally observed for muons with energy around a few GeV.

3.3. Measurements over the hemisphere

Fig. 11 shows the averaged values of the telescope counting rate as a function of both zenithal and azimuthal angles. Each point corresponds to a value averaged over one hour: the total acquisition time for these measurements is 72 h. No significant asymmetry of the muon flux distribution with respect to the azimuthal direction is observed for such a relatively short acquisition time of one hour per point.

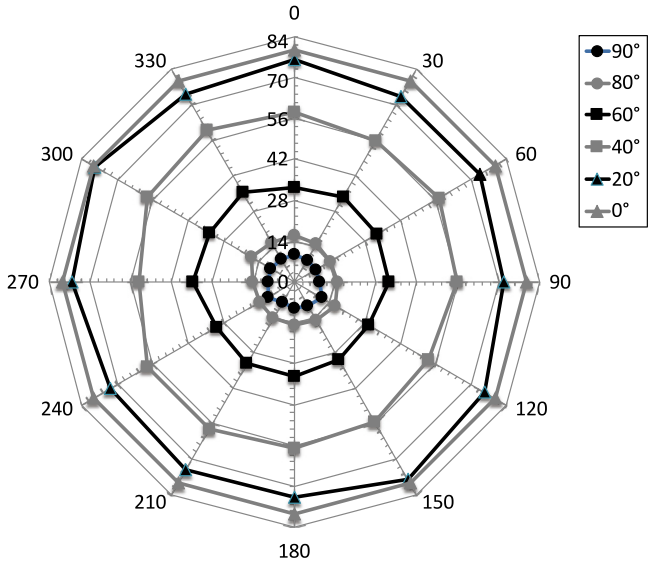

Fig. 11. Averaged values of the telescope counting rate as a function of both azimuthal (0–360°) and zenithal angles (0–90°). Each point corresponds to a value averaged over one hour. North direction has azimuth 0°, east 90°, south 180°, and west 270°; vertical direction has zenithal 0° and horizontal 90°. The radial scale shows the counting rate of the telescope.

4. Conclusion

In this paper we presented a muon telescope developed in this work to accurately characterize the flux of atmospheric muons at ground level as a function of both zenithal and azimuthal angles. The experimental setup, the control software and the calibration of the instrument have been described in detail. Through TRIM simulation work we have established that the telescope can detect incident muons with a minimum energy of 38 MeV in vertical incidence. We also presented a modeling of the counting rate of the telescope based on a model published in the literature. Our experimental measurements showed that the muon intensity in vertical incidence is $I_0 \approx 100$ m^{-2} s^{-1} sr^{-1}, in very good agreement with the values of the vertical flux reported in literature at this latitude. Then, we have finely characterized the dependence of atmospheric muon flux with the zenithal angle of the telescope and with the azimuthal direction. Raw measurements as well as the fitting of our model on experimental data showed a perfect square cosine dependence ($n = 2.0 \pm 0.1$) of the incident muon distribution, in excellent agreement with the value generally reported in the literature for energy muons ~3 GeV.

Acknowledgments

This work has been conjointly supported by France's General Directorates DGA and DGE, under convention #132906128 (EVEREST project).

References

[1] P.K.F. Grieder, Cosmic Rays at Earth, Elsevier Press, Netherlands, 2001.

[2] J.L. Autran, D. Munteanu, Soft Errors: From Particles to Circuits, Taylor & Francis/CRC Press, 2015, p. 439.

[3] D. Munteanu, J.L. Autran, Modeling and simulation of single-event effects in digital devices and ICs, IEEE Trans. Nucl. Sci. 55 (4) (2008) 1854–1878.

[4] S. Semikh, S. Serre, J.L. Autran, D. Munteanu, S. Sauze, E. Yakushev, S. Rozov, The plateau de bure neutron monitor: Design, operation and Monte-Carlo simulation, IEEE Trans. Nucl. Sci. 59 (2) (2012) 303–313.

[5] J.L. Autran, D. Munteanu, P. Roche, G. Gasiot, S. Martinie, S. Uznanski, S. Sauze, S. Semikh, E. Yakushev, S. Rozov, P. Loaiza, G. Warot, M. Zampaolo, Soft-errors induced by terrestrial neutrons and natural alpha-particle emitters in advanced memory circuits at ground level, Microelectron. Reliab. 50 (2010) 1822–1831.

[6] J.L. Leray, Effects of atmospheric neutrons on devices, at sea level and in avionics embedded systems, Microelectron. Reliab. 47 (2007) 1827–1835.

[7] J.L. Autran, S. Serre, D. Munteanu, S. Martinie, S. Sauze, S. Uznanski, G. Gasiot, P. Roche, Real-time soft-error testing of 40 nm SRAMs, in: 2012 Proceeding of the IEEE International Reliability Physics Symposium, IRPS, 2012, pp. 3C.5.1–3C.5.9.

[8] J.L. Autran, D. Munteanu, P. Roche, G. Gasiot, Real-time soft-error rate measurements: A review, Microelectron. Reliab. 54 (2014) 1455–1476.

[9] B.D. Sierawski, M.H. Mendenhall, R.A. Reed, M.A. Clemens, R.A. Weller, R.D. Schrimpf, E.W. Blackmore, M. Trinczek, B. Hitti, J.A. Pellish, R.C. Baumann, S.-J. Wen, R. Wong, N. Tam, Muon-induced single event upsets in deep-submicron technology, IEEE Trans. Nucl. Sci. 57 (6) (2010) 3273–3278.

[10] B.D. Sierawski, R.A. Reed, M.H. Mendenhall, R.A. Weller, R.D. Schrimpf, S.-J. Wen, R. Wong, N. Tam, R.C. Baumann, Effects of scaling on muon-induced soft errors, in: 2011 Proceeding of the IEEE International Reliability Physics Symposium, IRPS, 2011.

[11] L.W. Massengill, B.L. Bhuva, W.T. Holman, M.L. Alles, T.D. Loveless, Technology scaling and soft error reliability, in: 2012 Proceeding of the IEEE Reliability Physics Symposium, IRPS, 2012, pp. 3C.1.1–3C.1.7.

[12] P. Roche, J.L. Autran, G. Gasiot, D. Munteanu, Technology downscaling worsening radiation effects in bulk: SOI to the rescue, in: IEEE International Electron Device Meeting, IEDM, 2013, pp. 766–769.

[13] https://skyvision.fr/the-user-guide/dobson/ultra-compact-dobson/?lang=en.

[14] http://www.eljentechnology.com/index.php/component/content/article/31-general/48-ej-200.

[15] D.E. Groom, et al., At. Data Nucl. Data Tables 78 (2001) 183–356.

[16] J.F. Ziegler, J.P. Biersack, U. Littmark, The Stopping and Range of Ions in Matter, Pergamon, New York, 1985.

[17] H.H.K. Tang, SEMM-2: A new generation of single-event-effect modeling tools, IBM J. Res. Dev. 52 (2008) 233–244.

[18] T.R. Sanderson, D.E. Page, Geometrical aspects of the performance of cosmic ray detector telescopes in non-isotropic particle distributions, Nucl. Instrum. Methods 104 (3) (1972) 493–504.

[19] G.R. Thomas, D.M. Willis, Analytical derivation of the geometric factor of a particle detector having circular or rectangular geometry, J. Phys. E 5 (3) (1971) 261–263.

[20] J.D. Sullivan, Geometrical factor and directional response of single and multi-element particle telescopes, Nucl. Instrum. Methods 95 (1971) 5–11.

[21] S. Cecchini, M. Spurio, Atmospheric muons: Experimental aspects, Geosci. Instrum. Methods Data Syst. 1 (2012) 185–196.

[22] J.W. Lin, Y.-F. Chen, R.-J. Sheu, S.-H. Jiang, Measurement of angular distribution of cosmic-ray muon fluence rate, Nucl. Instrum. Methods A 619 (2010) 24–27.